AGU PUBLICATIONS

JGR

Journal of Geophysical Research: Earth Surface

RESEARCH ARTICLE
10.1002/2015JF003709

This article is a companion to *Hodge and Hoey* [2016] doi:10.1002/2015JF003706.

Key Points:
- Sediment patches tend to form in low-elevation, sheltered areas, but high flow velocities can override this
- At lower sediment supply, bed topography determines patch stability and patches are relatively insensitive to sediment supply
- At higher sediment supply, sediment patches stabilize by grain-grain and grain-flow interactions

Supporting Information:
- Supporting Information S1
- Movie S1

Correspondence to:
R. A. Hodge,
rebecca.hodge@durham.ac.uk

Citation:
Hodge, R. A., and T. B. Hoey (2016), A Froude-scaled model of a bedrock-alluvial channel reach: 2. Sediment cover, *J. Geophys. Res. Earth Surf.*, *121*, doi:10.1002/2015JF003709.

Received 27 AUG 2015
Accepted 22 JUL 2016
Accepted article online 29 JUL 2016

A Froude-scaled model of a bedrock-alluvial channel reach: 2. Sediment cover

Rebecca A. Hodge[1] and Trevor B. Hoey[2]

[1]Department of Geography, Durham University, Durham, UK, [2]School of Geographical and Earth Sciences, University of Glasgow, Glasgow, UK

Abstract Previous research into sediment cover in bedrock-alluvial channels has focussed on total sediment cover, rather than the spatial distribution of cover within the channel. The latter is important because it determines the bedrock areas that are protected from erosion and the start and end of sediment transport pathways. We use a 1:10 Froude-scaled model of an 18 by 9 m reach of a bedrock-alluvial channel to study the production and erosion of sediment patches and hence the spatial relationships between flow, bed topography, and sediment dynamics. The hydraulic data from this bed are presented in the companion paper. In these experiments specified volumes of sediment were supplied at the upstream edge of the model reach as single inputs, at each of a range of discharges. This sediment formed patches, and once these stabilized, flow was steadily increased to erode the patches. In summary: (1) patches tend to initiate in the lowest areas of the bed, but areas of topographically induced high flow velocity can inhibit patch development; (2) at low sediment inputs the extent of sediment patches is determined by the bed topography and can be insensitive to the exact volume of sediment supplied; and (3) at higher sediment inputs more extensive patches are produced, stabilized by grain-grain and grain-flow interactions and less influenced by the bed topography. Bedrock topography can therefore be an important constraint on sediment patch dynamics, and topographic metrics are required that incorporate its within-reach variability. The magnitude and timing of sediment input events controls reach-scale sediment cover.

1. Introduction

The spatial pattern of sediment cover in a bedrock-alluvial river is important in a range of different contexts. First, sediment cover protects the bed from erosion; the pattern of cover determines which parts of the bed are exposed to erosive processes and therefore has implications for incision rates and landscape evolution [*Sklar and Dietrich*, 2004; *Johnson and Whipple*, 2010]. Second, tracer experiments in a bedrock-alluvial channel demonstrate that grain travel paths are predominantly from one sediment patch to the next [*Hodge et al*., 2011]. Analogous to the role of riffles and pools in alluvial systems [e.g., *Pyrce and Ashmore*, 2003], the spatial pattern of sediment patches in bedrock-alluvial channels determines grain transport distances, as grains are preferentially deposited in sediment patches. Third, the contrast between alluvial and bedrock areas affects the critical shear stress for grain entrainment and consequently sediment transport [*Goode and Wohl*, 2010; *Hodge et al*., 2011]. Finally, both the spatial arrangement and stability of areas of sediment cover affect instream biota and these areas are potentially of greater ecological importance than continuous alluvial sediments [*O'Connor et al*., 2014]. This paper reports the use of a Froude-scaled physical model of a specific bedrock-alluvial channel to analyze the factors that control the spatial pattern and stability of sediment cover. This is the second in a pair of papers; the companion paper [*Hodge and Hoey*, 2016] demonstrates the Froude scaling of the model and quantifies relationships between the bed topography and hydraulics.

2. Background and Research Questions

Field observations [*Hodge et al*., 2011], flume experiments [*Chatanantavet and Parker*, 2008; *Hodge et al*., 2016], and theoretical analyses [*Hodge et al*., 2011; *Nelson and Seminara*, 2012; *Nelson et al*., 2014] have demonstrated that the most stable configuration of sediment on a bedrock surface is in patches, producing a spatial pattern of discrete alluvial and bedrock areas. Despite this, within-reach-scale patterns of sediment cover in bedrock-alluvial rivers have not received significant attention. From the perspective of incision and landscape evolution the focus has been on the total amount of sediment cover [e.g., *Sklar and Dietrich*, 2004; *Nelson and Seminara,* 2012; *Lague*, 2014] but not where that cover occurs within the channel. The rationale for this focus is that over long time

periods, there is negative feedback between local channel elevation, sediment cover, and erosion, and therefore, the bedrock incision and the locations of sediment cover will be averaged out across the reach; in this case the details at shorter timescales are unimportant. However, other flume experiments [e.g., *Johnson and Whipple*, 2007; *Finnegan et al*., 2007] have demonstrated positive feedback between the location of sediment and channel incision, in which case the spatial pattern of sediment cover could be important in determining the long-term morphological evolution. The first step in understanding these feedbacks, and evaluating the importance of within-reach-scale patterns, is to understand the controls on the location and stability of sediment cover.

Although incision models retain a reach-averaged focus, they increasingly include grain-scale processes. The grain-scale processes are often directly upscaled to the reach scale, ignoring the subreach-scale complexities of these systems [*Lague*, 2014]. Such grain-scale processes include grain saltation [*Sklar and Dietrich*, 2004], suspension [*Lamb et al*., 2008; *Scheingross et al*., 2014], the impact of grain-grain interactions on entrainment [*Hodge and Hoey*, 2012], the impact of differences in roughness between bedrock and alluvial surfaces on sediment cover [*Nelson and Seminara*, 2012; *Johnson*, 2014; *Inoue et al*., 2014], the impact of surface topographies on both sediment cover [*Chatanantavet and Parker*, 2008] and grain impact trajectories, and hence erosion rates [*Huda and Small*, 2014]. However, many of these processes will also be affected by the pattern of sediment cover within a reach; for example, saltation trajectories will be affected by the mixture of bedrock and alluvial surfaces that a saltating grain travels across, and channel roughness will vary spatially depending on the local bed morphology and sediment cover.

This paper uses a Froude-scaled model of a reach of a bedrock river to analyze the formation and erosion of sediment patches formed by discrete sediment pulses and to assess the extent to which these processes vary with sediment mass, discharge, and local bed topography. Our research questions are the following: (1) How does the amount of sediment cover vary with flow discharge and supplied sediment mass? (2) To what extent does bed topography control: (a) sediment patch location and (b) patch stability? (3) What are the relationships between sediment patch occurrence, hydraulics, and local bed topography?

The model was created using a novel combination of terrestrial laser scanning and 3-D printing. This model is Froude-scaled, which is an advance over previous models of bedrock-alluvial channels that have had Froude numbers significantly higher than are found in many bedrock channels [*Chatanantavet and Parker*, 2008; *Johnson and Whipple*, 2010]. Furthermore, the dimensions of the model (0.9 m wide) mean that spatially distributed hydraulics can be measured, and these data are presented in the companion paper [*Hodge and Hoey*, 2016]. Although these hydraulic data are mostly independent of the data presented here, they provide a useful approximation for the hydraulic conditions in these experiments; here rapidly changing flow and sediment cover prevented the collection of spatially distributed hydraulic data. The focus of our experiments is also different from previous physical models. *Chatanantavet and Parker* [2008] analyzed sediment cover from a reach-averaged perspective, considering the total amount of sediment cover, with only qualitative descriptions of where on the bed that sediment cover was developing. *Finnegan et al.* [2007] and *Johnson and Whipple* [2007] addressed the interactions between sediment cover and an eroding topography. Here a static topography is used, meaning that bed topography is independent of sediment and flow parameters.

3. Methods

3.1. Field and Flume Methods

The reach reproduced in the flume is an 18 m long section of Trout Beck, North Pennies, UK (54°41′35″N 2°23′18″W), which has an average width of 9 m, gradient of 0.02, and 22% sediment cover. The bedrock is Alston Formation Limestone, and the channel bed has a blocky topography with approximately horizontal bedding ~ 0.5 m thick, preferential erosion along vertical joints, vertical relief of up to 1 m, and a standard deviation of surface elevations of 0.12 m. (Figure 1a). Although the study reach does not have the extreme topography of some bedrock-alluvial channels, its topography is representative of many other channels (e.g., images in *Tinkler and Wohl* [1998], *Inoue et al.* [2014], and *Whitbread et al.* [2015]) Sediment has a D_{16}, D_{50}, and D_{84} of 23, 70, and 146 mm, respectively (where D_x is the grain size for which x% is finer; grain size distribution is shown in Figure 1c).

Terrestrial laser scanning, supplemented by differential GPS surveying of submerged areas of the bed, and 3-D printing were used to create a 1:10 Froude-scaled model of this reach of Trout Beck in the 8 m working length, 0.9 m wide flume at the University of Glasgow (Figures 1b and 1d). It was not feasible to remove the 22%

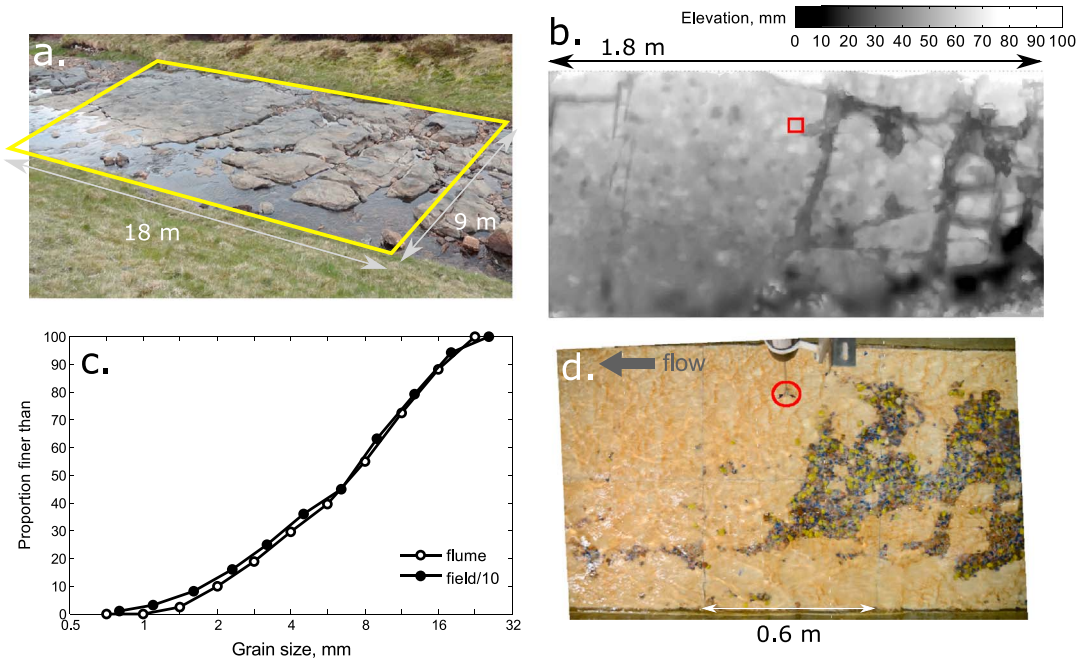

Figure 1. (a) The field location that was reproduced in the flume. (b) The 1:10 scale digital elevation model of the field reach bed topography created from terrestrial laser scanning and differential GPS data. (c) Grain size distributions for the field and flume sediment. Field data are downscaled by a factor of 10. (d) An image of the flume bed from run Q20/S16 (initial discharge of 20 L s^{-1}, 16 kg sediment pulse), showing sediment cover. The colored grains correspond to D_{16}, D_{50}, and D_{84}. The 0.6 m arrow indicates the width of one printed tile. The location of the Acoustic Doppler Velocimeter is circled in Figure 1d, and the area in which velocities and sediment cover were measured is the red square in Figure 1b.

sediment cover prior to surveying the reach, but this cover is mostly only a single grain thick. The presence of sediment cover indicates that this is a suitable reach for recreating sediment cover in the flume. The flume experiments indicate where additional sediment inputs to this channel would be deposited, but because of the different initial conditions, the experimental sediment patch locations cannot be compared to those in the channel. The printed surfaces, comprising six individual tiles, were installed in the flume 3.5 m downstream from the inlet, and the rest of the flume was filled with sediment of a comparable roughness to the printed bed. Full details of the model creation, and a comparison of flume and field data that demonstrates the Froude scaling, are presented in the companion paper [*Hodge and Hoey*, 2016].

Two sets of experiments were performed, focusing on hydraulics and sediment, respectively. In the first set (reported in the companion paper [*Hodge and Hoey*, 2016]), 3-D velocity data were collected from each of 18 locations, at discharges ranging from 20 to 60 L s^{-1}. These data show that hydraulic properties become more spatially variable as discharge increases and that a core of supercritical flow develops along the model domain. The hydraulic data from these 18 measurement locations give the following mean values and standard errors: Fr [0.88 ± 0.016 at Q = 20 L s^{-1} to 1.09 ± 0.019 at Q = 60 L s^{-1}]; (h/D_{84}) [2.74 ± 0.050 to 4.74 ± 0.054]; f [3.80 to 0.97]; and τ^* [0.067 ± 0.0012 to 0.116 ± 0.0013]. In these calculations, reach-averaged slope, S_l, has been used, Fr = Froude number, h = flow depth, f = Darcy-Weisbach roughness coefficient, and $\tau^* = (hS_l/1.65D_{50})$, assuming water and sediment densities of 1000 kg m^{-3} and 2650 kg m^{-3}, respectively.

In the second set of experiments (reported here), over a range of initial discharges, individual sediment pulses were introduced at the upstream end of the modeled reach so that the sediment formed sediment patches. Patch stability was then assessed by gradually increasing the discharge. These sediment experiments used a 1:10 scaled version of the field sediment, truncated at 1 mm, with D_{16}, D_{50} and D_{84} of 2.6, 7.3, and 14.8 mm, respectively, and subrounded grains. Only 4% of the original 1:10 scale grain size distribution was smaller than 1 mm (Figure 1c). In each run, the discharge was initially stabilized at a constant value; a specified quantity of sediment was input in a single pulse at the upstream end of the printed flume bed (using a board to disperse sediment evenly across the flume) and sediment patches formed. Five minutes after the sediment input, the discharge began to be increased at a rate of 0.7 L min^{-1} until a maximum discharge of 75 L s^{-1}

(maximum pump capacity) was reached. Two sets of data were collected during each run; a downward facing single-lens reflex camera took an image of the bed every 5 s, and 3-D acoustic Doppler velocimetry (ADV) data were collected at 25 Hz from a fixed location in the flume (Figure 1d). The ADV data show the impact of sediment cover on local hydraulics and are analyzed in the companion paper.

The sediment experiments used three different initial discharges (20, 35, and 50 L s^{-1}, denoted Q) and four different sediment masses (2, 4, 8, and 16 kg, denoted S) in the following combinations: Q20/S0, Q20/S2, Q20/S4, Q20/S8, Q20/S16, Q35/S4, Q35/S8, Q35/S16, Q50/S2, Q50/S4, and Q50/S8. The range of sediment masses and discharges was selected to cover a range of field conditions (20 L s^{-1} is equivalent to just below bankfull in the field setting) and to produce a range of sediment cover extents. Three further runs at Q20/S4 were completed; one replicate with the same sediment ($Q20/S4_{rep}$), one with coarse angular uniform 16 mm sediment ($Q20/S4_C$), and one with fine angular uniform 8.5 mm sediment ($Q20/S4_F$). The uniform sediment runs allowed the impact of sediment sorting and shape to be assessed. Comparison with experiments presented in *Hodge et al.* [2016], which quantified the stability of sediment patches of this uniform sediment on a flat bed, also allows assessment of the impact of the rougher topography in these experiments. Experimental duration was determined by the rate of changing discharge and ranged from 33 min to 85 min for experiments starting at 50 L s^{-1} and 20 L s^{-1}, respectively.

Camera images were processed in MATLAB to segment automatically the sediment patches from the background and thus produce a map of sediment cover. The segmentation technique used the red channel in the RGB image as this had the greatest contrast between the bed and sediment. First, a background model from initial images of the flume bed without sediment cover was produced by averaging 12 images. Sediment was then identified as areas where the pixel values decreased relative to the background model. The background model was updated to account for changes in water depth throughout each experiment. Further filtering removed noise caused by the water surface. A video of run Q20/S16 (Movie S1 in the supporting information) shows the results of the segmentation algorithm and the dynamics of an experimental run. Errors associated with changes in pixel location produced by refraction at different water depths were minimal compared to other segmentation errors and were not corrected for.

Sediment cover maps were produced at 1 min intervals for each run. The segmentation algorithm was tested through comparison with a total of 28 manually segmented images, comprising up to 10 images from each of three runs (Q20/S2, Q20/S8, and Q20/S16). The Jaccard index (J) was used to calculate the similarity between the manual and automatic segmentation, where the index of two areas, A (manually segmented sediment) and B (automatically identified sediment), is

$$J(A,B) = |A \cap B| / |A \cup B| \quad (1)$$

J accounts for the location as well as the amount of sediment cover. Values range between 0 and 1, values closer to 1 indicating a higher correlation between the two images. The mean (and range) of J values for each set of images from a flume run are Q20/S2, 0.68 (0.62 to 0.77); Q20/S8, 0.76 (0.70 to 0.84); and Q20/S16, 0.84 (0.74 to 0.91). Much of the dissimilarity between the manual and automated segmentations occurs around patch edges and in small patches which are either missed or erroneously identified by the automatic segmentation. Consequently, J values are higher when there is more sediment cover because these errors comprise a smaller proportion of the total area. For further illustration, absolute differences between manual and automatically segmented sediment cover range from 0.1 to 2.4 % of the total image area, with a root-mean-square (RMS) error of 0.9%, and tend to decrease as sediment cover decreases.

Images and sediment cover maps were registered to a common coordinate system using a series of 12 markers on the tiles; the RMS of the registration errors was 6.4 mm. This enables sediment cover to be correlated with bed topography. Sediment cover maps and the bed topography model were resampled onto a 5 mm grid to ensure comparable and spatially uniform data sets. A time-discharge rating curve was used to calculate the discharge in the flume during each of the sediment cover maps.

The final component of the methods is a simple numerical model designed to provide a control condition in which patches develop independent of any interaction with the flow. Such an approach has been used to estimate reach-scale sediment cover [*Inoue et al.*, 2014]. This space filling model determines the sediment cover produced by filling up the channel bed topography. The cells of the digital elevation model were virtually filled, starting from the lowest cell and adding cells in order of increasing elevation. Throughout

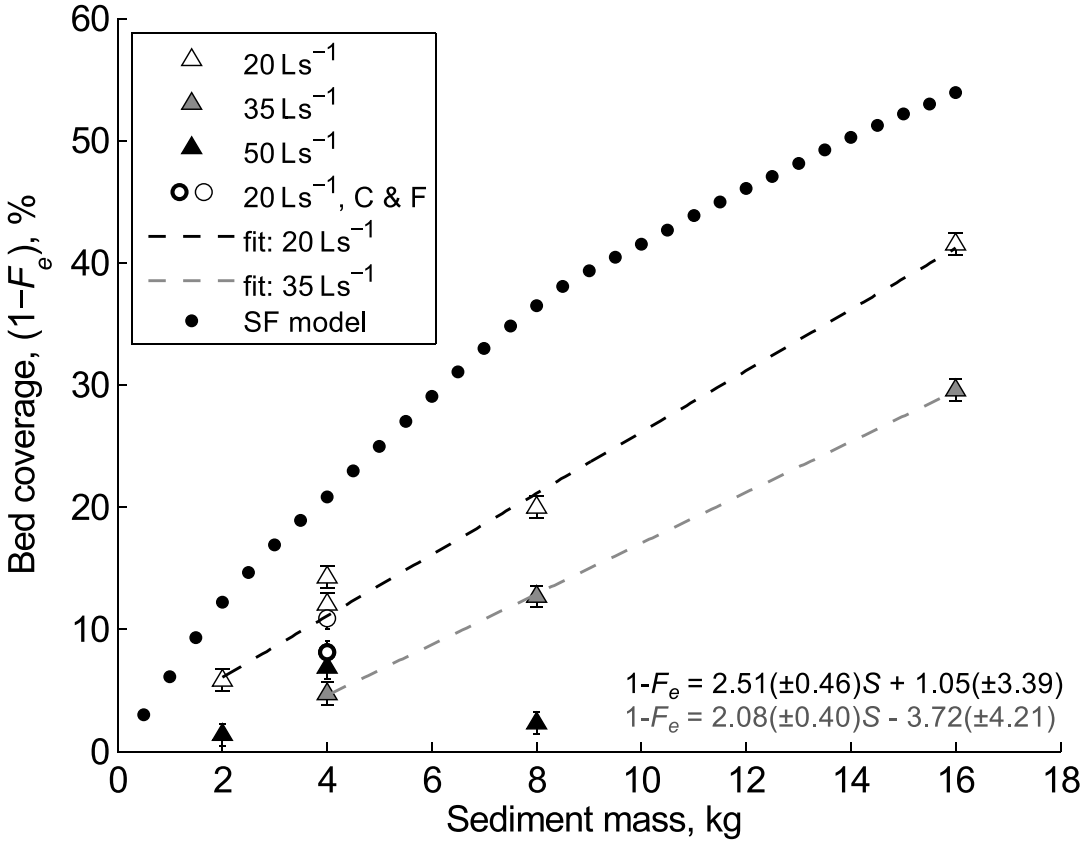

Figure 2. Percentage of bed with sediment cover ($1 - F_e$, where F_e is bedrock exposure) at 4.5 min after sediment input into the flume. Circles are coarse and fine uniform sediments. Error bars are the 0.9% root-mean-square error between manual and automated segmentations. Black dots are predictions of sediment cover from an elevation-based space filling model. Linear regressions fitted to data are as follows, where S is sediment mass: all data: $1 - F_e = 2.11(\pm 0.81)\ S - 0.54\ (\pm 6.38)$, $R^2 = 0.75$; $Q = 20\ L\ s^{-1}$ (including coarse and fine sediment): on figure, $R^2 = 0.98$; $Q = 35\ L\ s^{-1}$: on figure, $R^2 = 0.99$. Stepwise regression of sediment mass and discharge against sediment cover, for all mixed sediment size experiments, gives: $1 - F_e = 2.07S - 0.34Q + 10.20$, $R^2 = 0.88$.

the process, the sediment surface elevation was the same in all sediment-containing cells; this assumption is not necessarily true in the field and flume. Filling continued until the volume of virtual sediment was equal to a specified mass (assuming a density of $2.65\ g\ cm^{-3}$ and porosity of 0.3).

4. Results

4.1. The Extent and Spatial Pattern of Initial Sediment Cover

Initial patterns of sediment cover are analyzed 4.5 min after the sediment injection, prior to the subsequent increase in flow. Figure 2 shows linear relationships between the proportion of the flume bed covered by sediment and the mass of sediment that was added to the flume for both $Q = 20\ L\ s^{-1}$ and $Q = 35\ L\ s^{-1}$. At $50\ L\ s^{-1}$, transport was more intense and less sediment was retained in the modeled section. The latter experiments do not follow a linear relationship due to an anomalously high cover in run Q50/S4 which may be the result of the backwater from the flume tailgate extending up to the downstream end of the tiles in this run.

For $Q = 20\ L\ s^{-1}$, $Q = 35\ L\ s^{-1}$, and for all data combined, the gradients of the relationships between sediment mass and cover are not significantly different (95% confidence; see Figure 2 for values). There is systematic variation in the intercept (albeit not at a 95% confidence interval), which results in higher discharges producing lower cover. Stepwise regression of cover against sediment mass and discharge indicates that both significantly contribute to the relationship, with respective p values of < 0.001 and 0.003. The initial sediment cover in the runs with uniform coarse and fine sediment ($Q20/S4_C$ and $Q20/S4_F$) was 8.1 and 10.9%,

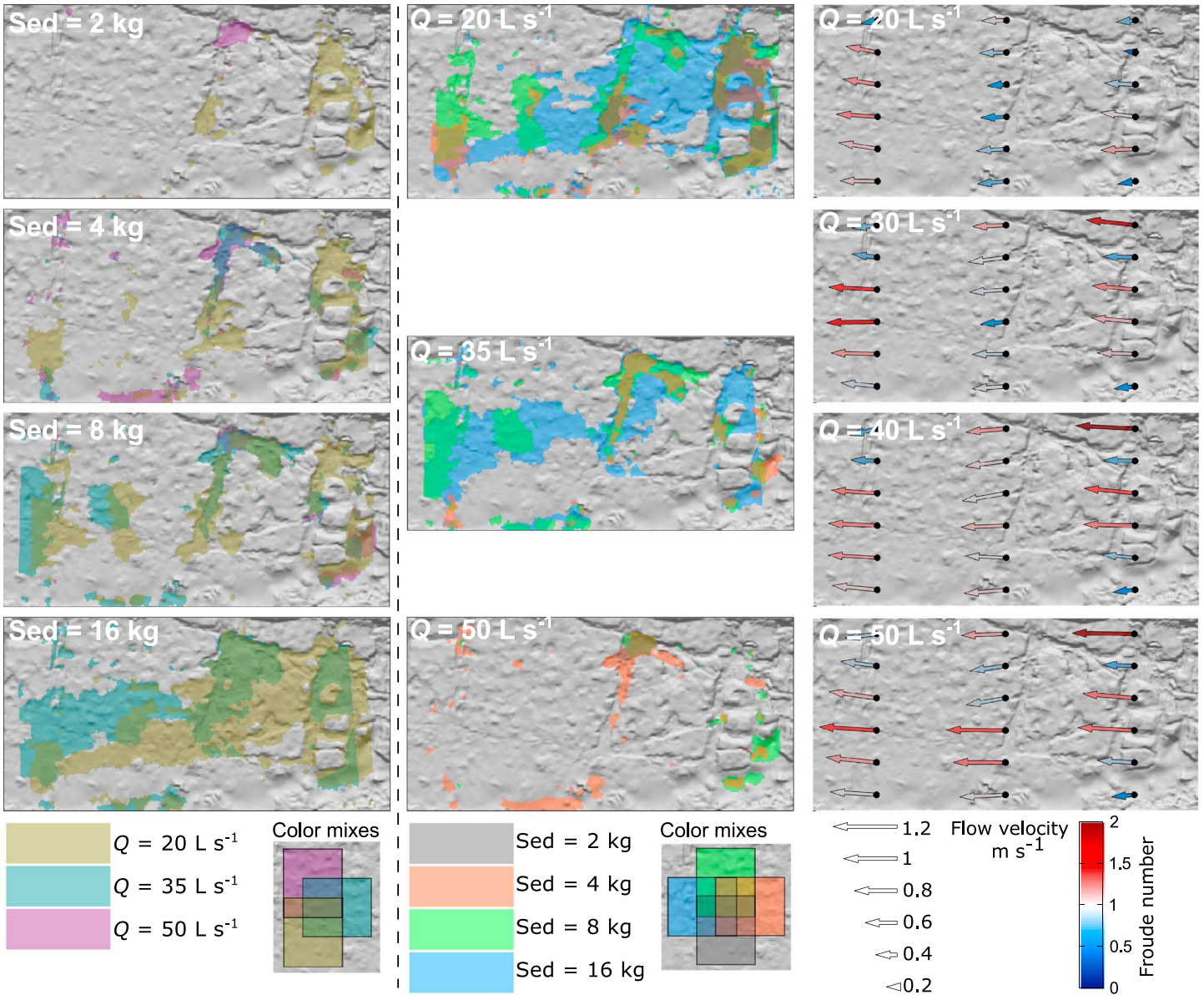

Figure 3. Overlays of initial sediment cover for runs with the (left column) same sediment mass or (middle column) same initial discharge. Colors are transparent, so mixture panels show how the colors combine. Data are for all runs with mixed sediment sizes. Bed area is 1.8 m long by 0.9 m wide. Sediment patches are truncated within about 50 mm of upstream and/or downstream ends because the photos did not cover the entire length of the test section. Flow velocities and Froude numbers measured at 18 locations across the flume are also shown for (right) a range of discharges (see companion paper [*Hodge and Hoey*, 2016] for further details). Note that the velocity data were collected with no sediment in the flume and therefore are only illustrative of the conditions during the sediment runs.

respectively, which is consistent with the trend of the $Q = 20\ \mathrm{L\,s^{-1}}$ runs; adding or removing these data makes no significant difference to the regression in Figure 2.

Despite the differences in sediment mass and discharge, there are similarities between the locations of sediment cover (Figure 3); 47.5% of the flume bed area never had initial sediment cover, whereas 1.2% had initial sediment cover in at least 10 out of the 13 experiments. For runs with the same initial discharge but different sediment masses, there is persistence in the location of the initial sediment patches. For almost all runs, at least 70% of the locations that are initially sediment covered in one run also have sediment cover in subsequent runs with higher sediment masses but the same initial discharge. The main differences in sediment location are caused by changes in initial discharge. At initial discharges of 20 and $35\ \mathrm{L\,s^{-1}}$, sediment patches form in low-elevation areas at the upstream end of the reach. However, at an initial discharge of $50\ \mathrm{L\,s^{-1}}$,

sediment is preferentially deposited in depressions further downstream. Figure 3 shows how velocities in the upstream transect increased at high discharges, inhibiting sediment deposition. Furthermore, sediment was introduced to the flume <0.3 m upstream of these areas and at higher discharges would have acquired a larger downstream velocity so overpassing the upstream areas of the bed.

4.2. Topographic Controls on Initial Sediment Cover

Although some sediment is deposited at most elevations across the entire modeled reach, the majority of sediment is deposited on lower elevation areas of the bed. As the volume of sediment increases, in experiments with initial discharge of 20 and 35 L s^{-1}, the mean elevation of sediment covered areas increases from 31 to 39 mm (Q20/S2 to Q20/S16) and from 30 to 40 mm (Q35/S4 to Q35/S16) (Figure 4). Runs at 50 L s^{-1}, however, display the inverse pattern, with a drop in mean bed elevation as sediment mass increases from 2 to 8 kg; this pattern is related to the different locations of sediment deposition under a higher discharge (Figure 3). Bed elevation therefore seems to be an important, but not the only, control on sediment cover location.

Analysis of the hydraulic data in the companion paper shows that at $Q = 20$ L s^{-1}, there was a negative correlation between downstream velocity and a topographic index, Δ_z. Δ_z is the difference between the local bed elevation and the maximum elevation over an upstream and lateral distance of 300 and ± 30 mm, respectively; these distances produced the highest correlations between topography and velocity [*Hodge and Hoey*, 2016]. Relationships between velocity and bed elevation were not significant. Initial sediment cover in runs with $Q = 20$ and 35 L s^{-1} is typically deposited in areas of the bed that are lower and have a higher Δ_z (Figure 4). As the sediment pulse mass increases, the cover extends to higher elevations and lower Δ_z. Consequently, both elevation and Δ_z appear to influence the sediment location at initial discharges of 20 and 35 L s^{-1}.

The extent to which bed elevation determines the location of sediment patches is evaluated by considering the spatial pattern of sediment cover that is produced by the space filling model. The relationship between the input sediment mass and the depositional area predicted by the space filling model is compared to experimental data in Figure 2. The model predicts a curved relationship between sediment mass and area, with areas significantly greater than observed in the experiments. For example, 4.5 kg of sediment in the space filling model produces 23% sediment cover, whereas in flume run Q20/S8, 8 kg of sediment produces 20% sediment cover. The larger model predictions occur in part because an unknown amount of the sediment added in each run was transported out of the experimental section without being deposited in a sediment patch. It would thus be appropriate to shift the entire space filling model curve to the right in Figure 2, but the trapping efficiency of the bed, whether this varies with input volume and hence the magnitude of the shift, is unknown. Sediment becomes more spread out in the flume experiments than in the space filling model as the volume of sediment introduced increases (Figures 2 and 5). This slower lateral expansion in the space filling model is confirmed by a power law fit to sediment cover predictions, which has an exponent of 0.68 (±0.029), indicating that as sediment mass increases, sediment area increases at a slower rate in contrast to the linear fit to the flume data.

In addition to the differences in measured and predicted total cover, the space filling model is also a poor predictor of the elevation and location of sediment patches (Figures 4 and 5). The maximum elevation predicted by the space filling model is similar to the mean elevation of the flume data (Figure 4), indicating that sediment is deposited at relatively higher elevations in the flume. Furthermore, the single elevation predicted by the model omits all the variability in the flume data. The space filling model correctly identifies some topographic depressions where sediment collects, but it also over predicts the occurrence of patches along one side of the flume (Figure 5). The elevation is relatively low along this side of the flume, but the flow velocities are comparatively high (see Figure 3 and companion paper); consequently, this is not a site of sediment deposition in the experiments. Alternative variants on the space filling model that also incorporated values of Δ_z did not produce better predictions of sediment patch location.

Using results from both the space filling model (Figures 2 and 5) and the measured hydraulics (Figure 3), both bed elevation and Δ_z are important factors affecting sediment patch location, but neither is sufficient to predict it. The spatial pattern of flow also needs to be considered, noting that this will itself vary with sediment cover.

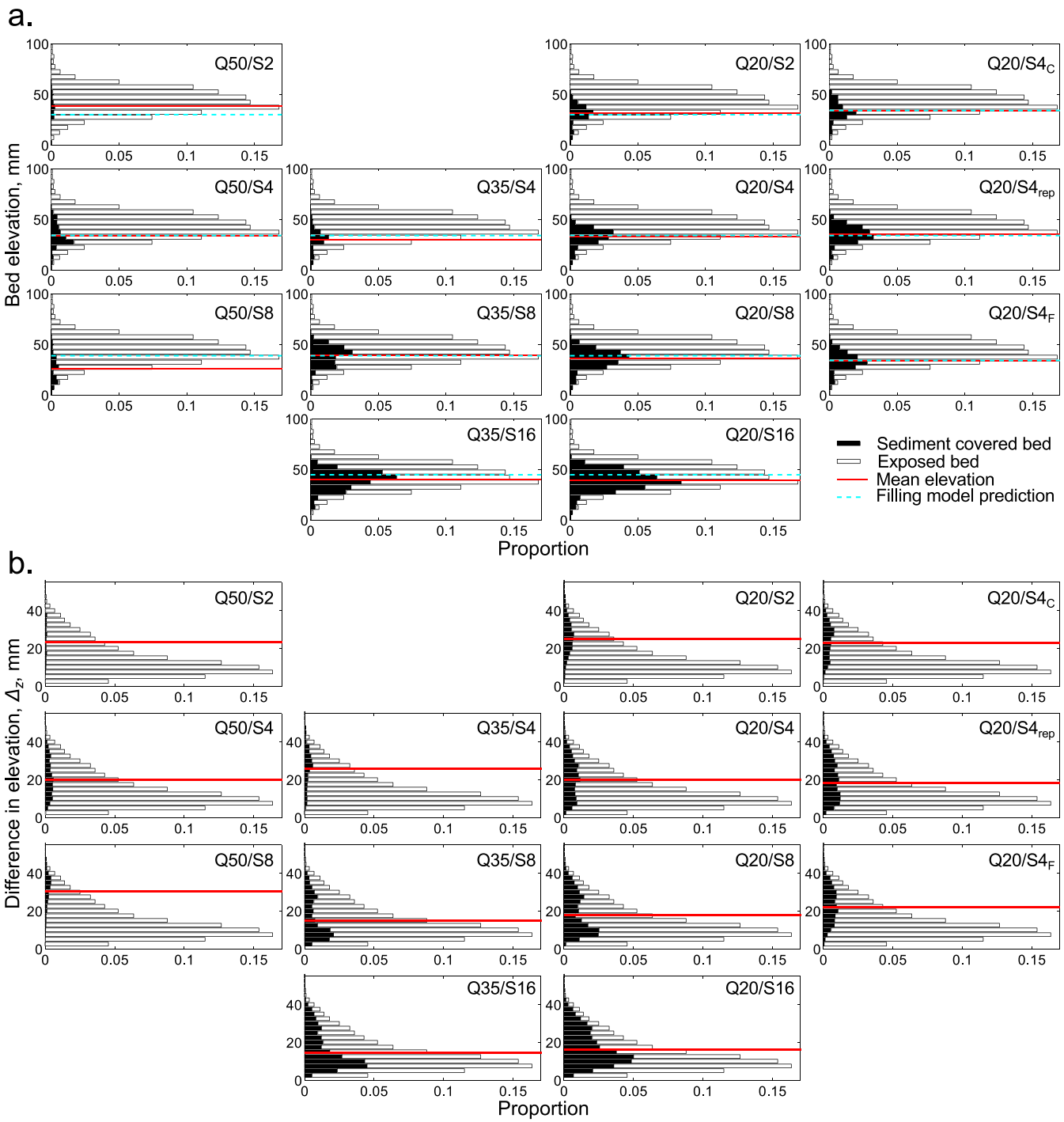

Figure 4. In each subplot, white bars show the distribution of either (a) bed elevation or (b) Δ_z across the entire bed. Δ_z is the difference between local and maximum upstream bed elevation over a 300 mm distance. Black bars show the distributions of these two properties for areas of the bed that had initial sediment cover in each run. The red line shows the mean elevation or Δ_z for all covered areas of the bed. Dashed cyan lines show the maximum elevation of the sediment cover produced by the same mass of sediment and a simple space filling model.

4.3. Length Scale of Initial Sediment Cover

The length scale of the initial sediment cover was analyzed by calculating the distances between all pairs of pixels that contained sediment; distributions of these distances are shown in Figure 6 for runs Q20/S2 through Q20/S16. Results from a random distribution of sediment cover are also shown for comparison; a random

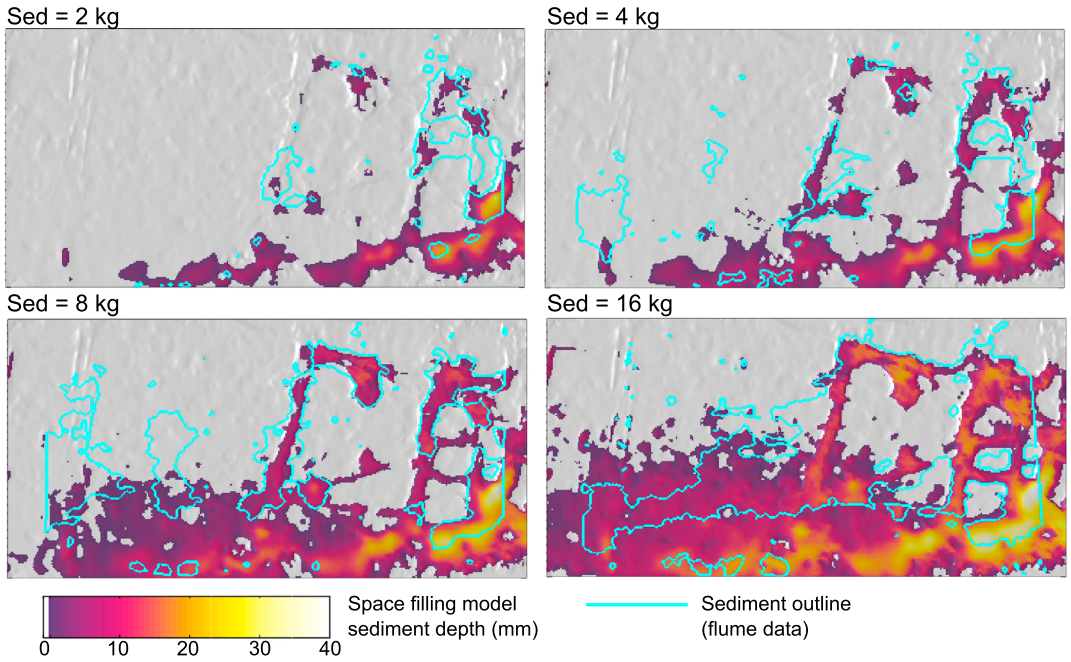

Figure 5. Locations and depths of sediment patches predicted by a simple space filling model. Sediment outlines show location of initial sediment patches in experiments with $Q = 20\,\mathrm{L\,s^{-1}}$ and the same mass of sediment (outlines are the same data as shown in Figure 3). Flow is from right to left. Bed area is 1.8 m long by 0.9 m wide. Experimental sediment patches are truncated within ~50 mm of upstream and/or downstream ends because the photos did not cover the entire length of the test section.

distribution would be expected in the case that there was no influence of the topography (nor grain-grain interactions). In Q20/S2, the modal distances are between 90 and 210 mm, with a secondary peak at 670 mm, and the distribution is different from a random arrangement of grains. The primary and secondary peaks likely correspond to distances between grains in the same patch and in different patches, respectively. These peaks are still present in Q20/S4, but the first peak is smaller and there is an additional peak at 1430 mm. The first and last peaks show the biggest difference from a random distribution. At Q20/S8 there are multiple peaks, although the overall trend is not dissimilar to a random distribution. At Q20/S16 there is a smooth distribution with a mode at 370 mm; the shape is similar to a random distribution, although the mode is at a shorter length. These distributions demonstrate how, as sediment volume increases, the sediment cover transitions from being clustered to being evenly distributed across the entire bed.

The spatial scales at which the sediment is clustered are similar to those identified in the companion paper as being a characteristic length scale of the bedrock topography (150 mm, Figure 6e). The topographic roughness of the flume bed varies as a function of the scale at which it is measured. Roughness was defined as the standard deviation of bed elevations (σ_z) [e.g., *Finnegan et al.*, 2007; *Johnson and Whipple*, 2007; *Inoue et al.*, 2014] and calculated using a moving window. As window sizes increase up to about 150 mm, there is a rapid increase in the mean value of σ_z (Figure 6e). At larger window sizes the mean continues to increase but at a slower rate. A semivariogram analysis of bed elevations in the downstream direction also reaches a sill value at about 150 mm. These results suggest that a window size of 150 mm is the minimum required to capture the topographic complexity of the bed and as such may represent a horizontal length scale for the bedrock topography and consequently may also be linked to the dimensions of sediment patches.

4.4. Erosion of Sediment Cover

Analysis of the formation of sediment cover has demonstrated the importance of both topography and flow in determining the location of sediment patches. After 5 min of steady flow in which sediment patches formed, the discharge was steadily increased to assess the patch stability. In most runs, sediment cover remained relatively constant until a discharge of between 30 and $35\,\mathrm{L\,s^{-1}}$, at which point cover started to

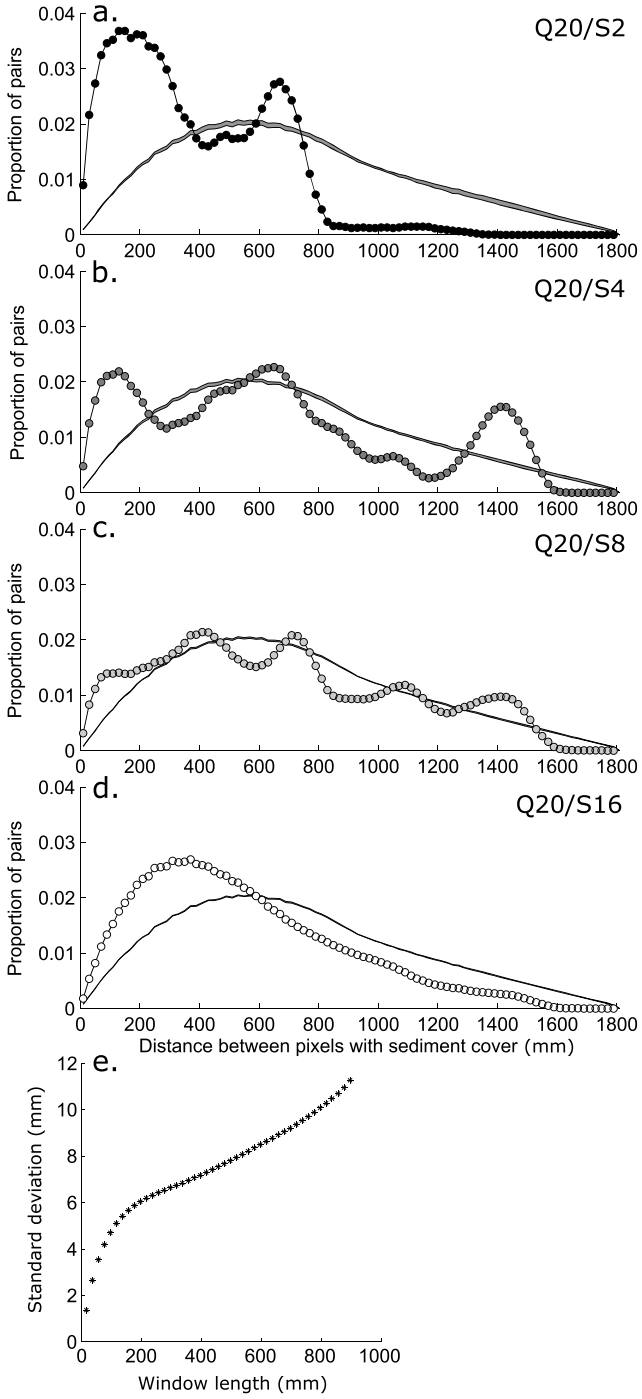

Figure 6. (a–d) Distributions of the distances between each pixel that contains sediment and every other sediment containing pixel. Data are from runs Q20/2 through Q20/16. Grey bands show the 95% confidence interval calculated from spatially random distributions of the same numbers of grains. (e) Mean of the standard deviation of elevations (σ_z) calculated from the bedrock topography, using moving windows of different lengths. The data in Figure 6e are taken from Figure 8 in the companion paper.

decrease as the patches began to be entrained (Figure 7a). Run Q20/S16 has an initial increase in sediment cover, because as sediment starts to be mobilized, it initially is more spread out over the bed before starting to be removed from the test section.

The patterns of decrease in sediment cover broadly fall into three regimes, depending on the mass of the sediment pulse. The first regime comprises runs with 2 kg pulses, with Q35/S4 also showing the same trend. The second regime comprises all other 4 kg and the 8 kg runs, and the final regime comprises the 16 kg runs. The similarity between the 4 and 8 kg runs is in contrast to the differences in initial sediment cover between these runs. The excess sediment cover in the 8 kg runs is quickly eroded once the flow starts to increase, collapsing the erosion curve onto that of the 4 kg runs. The decreases in sediment cover are a mixture of gradual decreases and steps, suggesting grain-by-grain removal of sediment from around patch edges and rapid destabilization of an entire sediment patch, respectively.

For each of the experimental runs, the discharge at which sediment cover in different locations was eroded is shown in Figures 8a to 8m. These figures are produced by mapping the maximum discharge at which each section of the bed surface was last covered with sediment (termed the threshold discharge, Q_t). Consequently, the maps of Q_t give an indication of the stability of sediment patches in different locations. Some sediment is redeposited and subsequently remobilized during the run, and so some sediment patches form during the experiments as a result of upstream sediment entrainment. In these maps of Q_t the bed tends to be segmented into distinct areas, with relatively abrupt transitions between areas with different threshold discharges (Figures 8a to 8m). This indicates that areas of sediment patches are removed in single erosional events; visual analysis of the experiment showed that this process was often initiated by entrainment of one or two key grains, which destabilized the surrounding patch. Such a process has also

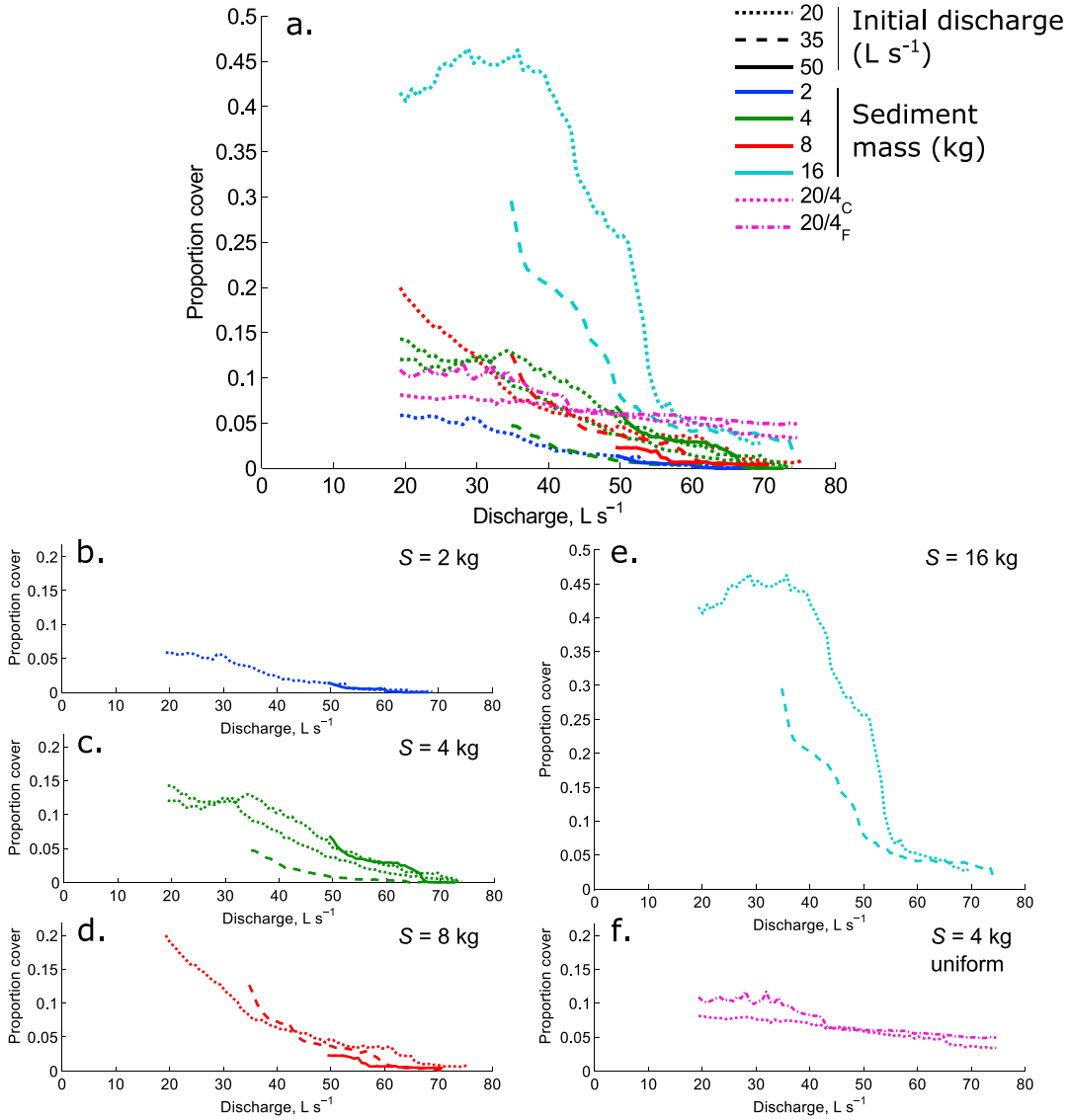

Figure 7. (a) Time series of total sediment cover from all experiments. (b–f) Subplots show the same data but separated out by sediment volume and grain size. The run conditions are indicated by the combination of color (sediment mass) and line style (initial discharge). Sediment cover is normalized by the area of the flume that was visible in the photos. Figure 7c shows the consistency in behavior of the two repeat runs with Q20/S4.

been observed for sediment patches on a flat bed [*Hodge et al.*, 2016]. Patch shrinkage through grain-by-grain removal around the edge seems to be less common, although the colored fringes around some of the more stable patches and across some of the widespread initial cover in Figures 8a to 8m indicate that it does occur. The relatively gradual decrease in cover shown in Figure 7 therefore hides the fact that at any one time, sediment is sourced from distinct areas of the bed rather than from across the entire bed.

For each run we calculate $\overline{Q_t}$, which is the mean of Q_t, (i.e., for Figures 8a to 8m, it is the mean of all of the displayed discharges). $\overline{Q_t}$ for each run varies with sediment mass and initial discharge (Figure 8q). There is an increase in $\overline{Q_t}$ of ~ 2 L s^{-1} when sediment mass increases from 2 to 4 kg. In contrast, values of $\overline{Q_t}$ for 4 and for 8 kg of sediment are very similar to each other, indicating that doubling the volume of sediment in the flume does not make the sediment patches more stable. For the 20 L s^{-1} runs, increasing the sediment mass from 8 to 16 kg produces a further increase in $\overline{Q_t}$ of 6 L s^{-1}, indicating that the sediment patches become more stable. This increased stability is not seen in the 35 L s^{-1} runs.

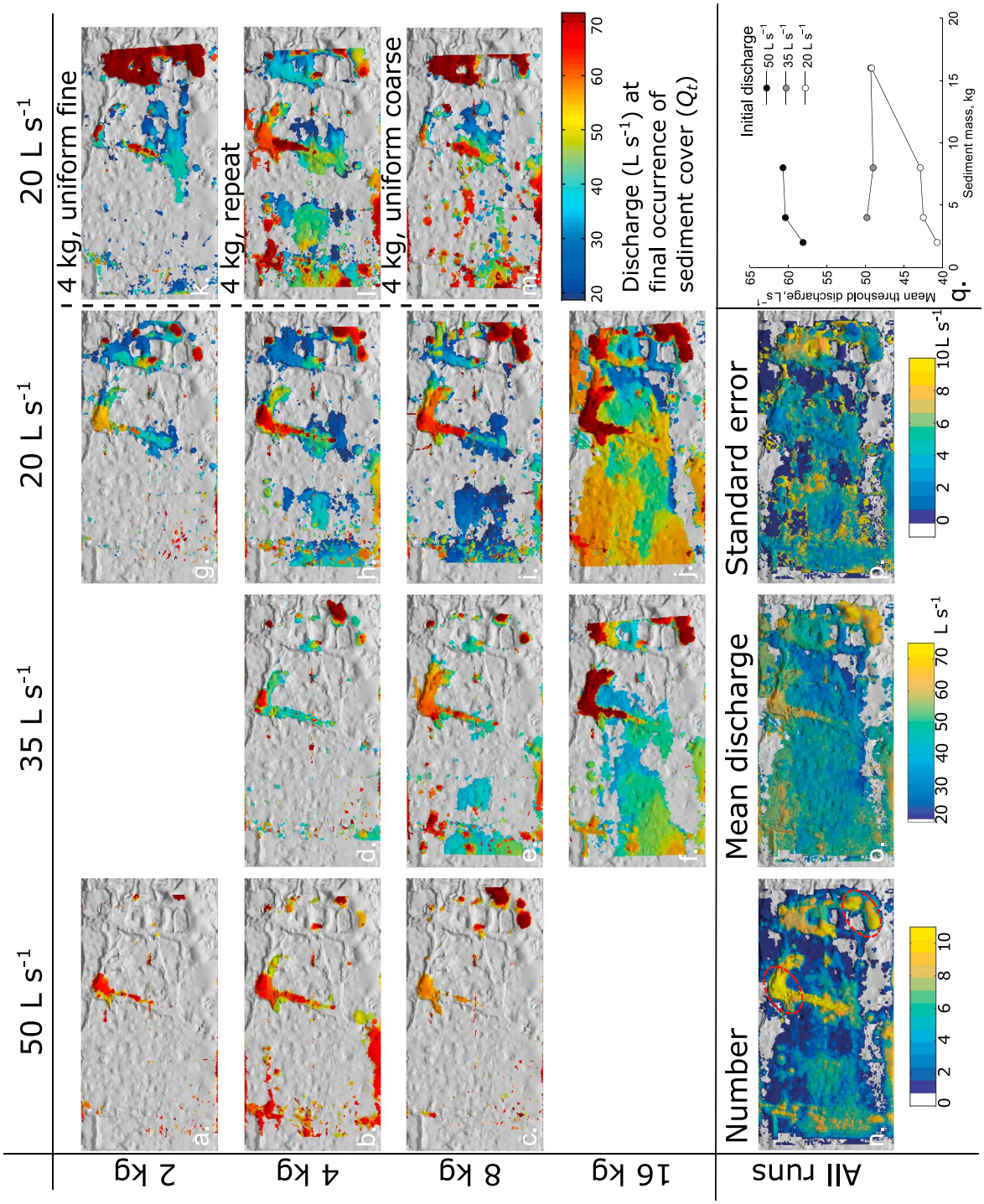

Figure 8. (a) to (m): Maps of discharge at which sediment is last present (threshold discharge, Q_t) at each location across the flume bed. Grey indicates no sediment cover at that location during that run. The sediment cover map includes all areas of the bed that contained sediment cover at any point during the run, not just sediment cover after the initial 5 min. Panels are arranged by initial discharge and sediment mass. Flow is from right to left. Bed area is 1.8 m long by 0.9 m wide. (n) The number of runs with sediment cover in each area of the bed; (o) the mean flow to remove sediment cover; (p) the standard error of the mean. Data are from all experiments, including the (k and m) two runs with uniform sediment. In Figure 8n, red ovals identify areas of persistent sediment cover, the elbow feature on the channel right, and the upstream pool on the left. The inset graph in Figure 8q shows the mean threshold discharge for each run (i.e., the mean of all discharges shown in Figures 8a to 8m.).

Figures 8n to 8p compile spatial data of sediment cover from all 13 experiments; although the experiments do have varying masses of sediment and initial discharges, the combined set identifies the consistent features in the deposition and erosion of sediment cover. There is persistence in sediment patch location between runs, with sediment patches most consistently occurring in the low areas of the bed around the upstream blocks; in particular, the "elbow" feature and upstream pool (circled in red in Figure 8n). The stability of sediment cover within these locations is also demonstrated by the high mean values of Q_t at which these sediment patches are eroded (Figure 8o). The standard error of Q_t in these locations is relatively low (Figure 8p), indicating similarity between runs. Other areas of the bed display a far higher standard error of Q_t hence greater variation between runs.

Patches formed from uniform sediment are more stable than those in most of the mixed sediment runs. All of the mixed sediment patches decreased in extent with increasing discharge, but the uniform sediment patches show little erosion (Figure 7, 8k, and 8m). The uniform runs have the highest sediment cover at the end of the experiment, with only the mixed 16 kg runs having similar levels of cover. The spatial pattern of Q_t (Figures 8k and 8m) shows that sediment patches of uniform grains form in some of the same places as in the mixed sediment runs but that there are additional locations where uniform sediment patches are more stable than mixed sediment patches. Both uniform sediments are comprised of angular grains (0.2 on the Krumbein roundness scale) [*Krumbein*, 1941], compared to the typically subrounded sediments of the mixed sediment (0.5 on the Krumbein scale). The results suggest that grain shape can affect grain-grain and grain-bed interactions and hence patch stability.

4.5. Topographic Controls on the Erosion of Sediment Cover

Both bed elevation and Δ_z were found to influence the initial location of sediment cover (Figure 4); Figure 9 shows how both of these properties also influence values of Q_t. There is a general tendency for sediment stability to increase at lower elevations; however, both stable sediment and unstable sediment that is eroded first come from a wide range of elevations. Sediment is also more stable at higher values of Δ_z, with a more consistent pattern of increased stability than is shown for elevation.

The similarities between Q20/S4 and Q20/S8 again demonstrate that they have a similar regime, despite differences in their initial sediment cover. This similarity is because the extra sediment that is deposited in Q20/S8 is soon eroded. Run Q20/S16 shows relatively stable sediment cover in locations that have both a high elevation and low value of Δ_z, indicating that another factor (likely grain-grain interactions) is increasing its stability. The uniform sediment runs also show higher stability across a wider range of elevations and Δ_z than the mixed sediment runs, again suggesting that interactions between these angular grains are stabilizing the sediment patches.

The discharge at which sediment is introduced is also important. The small amount of sediment that is deposited in runs Q50/S8 is only deposited in very stable areas of the bed. Sediment introduced at a lower discharge tends to be more stable at a higher discharge, whereas sediment that is put into the flume at that higher discharge is unable to form stable sediment patches. This may be because sediment that is already in the flume influences the local hydraulics and/or exhibits greater stability through grain-grain interactions; consequently, the relative timing of sediment supply and flow events is also an important control on sediment stability.

4.6. Relationships Between Sediment Cover, Flow Velocity, and Bed Topography

The relative importance of topography and hydraulics can be ascertained through a comparison of the sediment erosion data set with the hydraulic data collected in the runs without sediment cover (presented in Figure 3 and *Hodge and Hoey* [2016]). These two data sets are independent and therefore not strictly comparable as the hydraulic data do not include the changes in local roughness and velocity caused by the sediment cover (as demonstrated in *Hodge and Hoey* [2016]). However, on the assumption that the presence of sediment increases roughness and so will decrease velocities, the hydraulic data can be used as an upper estimate. Over all discharges, Figure 10a shows a significant negative relationship ($p < 0.001$) between downstream velocity and the proportion of runs with sediment cover. Δ_z and elevation produce significant positive ($p = 0.002$) and weakly significant negative ($p = 0.06$) relationships, respectively (Figures 10b and 10d). Reynolds stress (Figure 10c) and σ_z (calculated using a 150 mm window) do not produce significant relationships. Using the data from all discharges, stepwise regression of the proportion of runs with sediment

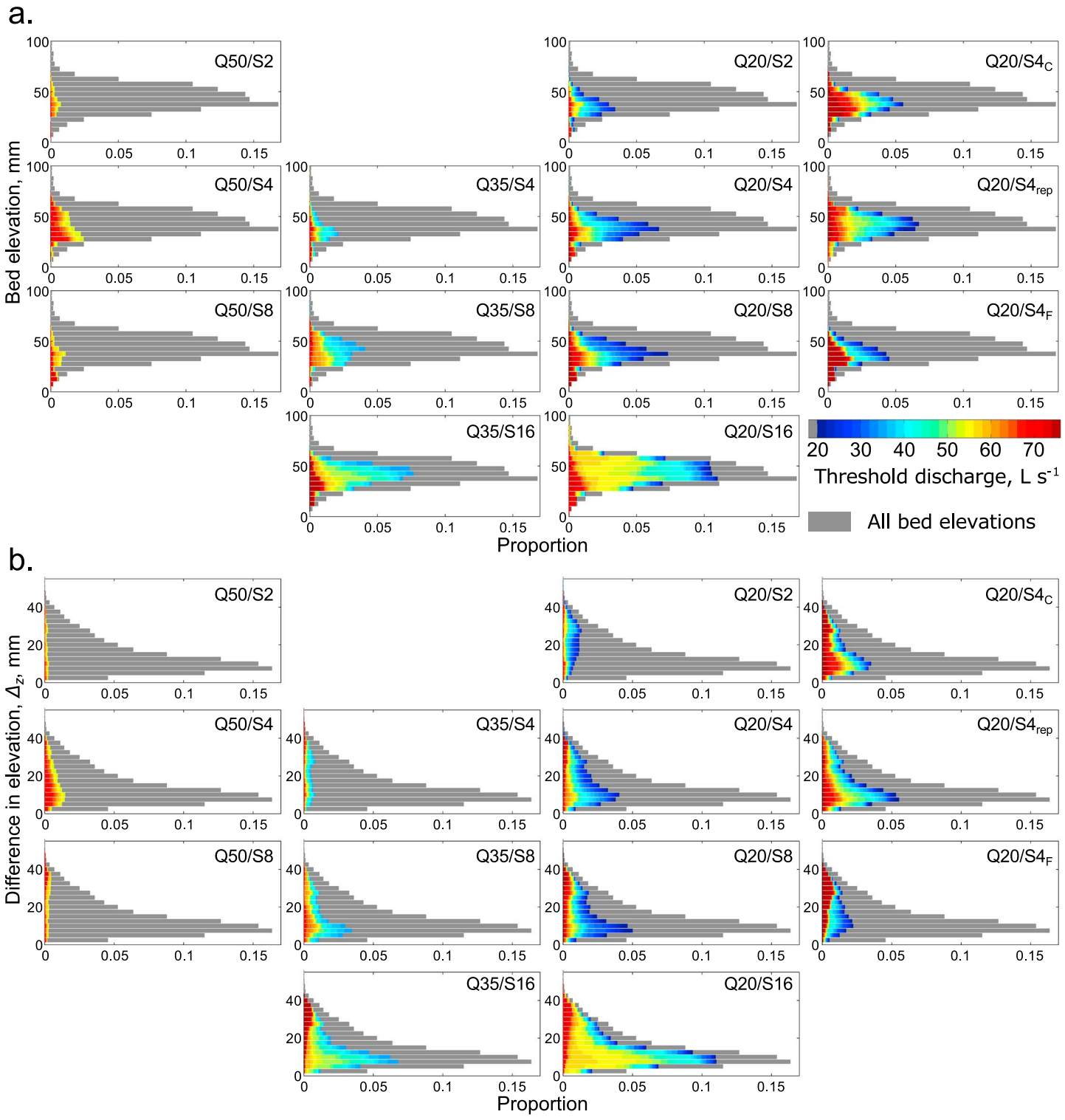

Figure 9. The threshold discharge (Q_t) at which sediment was eroded related to (a) bed elevation and (b) Δ_z. Δ_z is the difference between local and maximum upstream bed elevation over a 300 mm distance. In each panel, grey bars show the distribution of either bed elevations or Δ_z. Colored bars show the proportion of each elevation or value of Δ_z that was covered in sediment during that experimental run, and the colors show the discharge at which that sediment was eroded (Q_t).

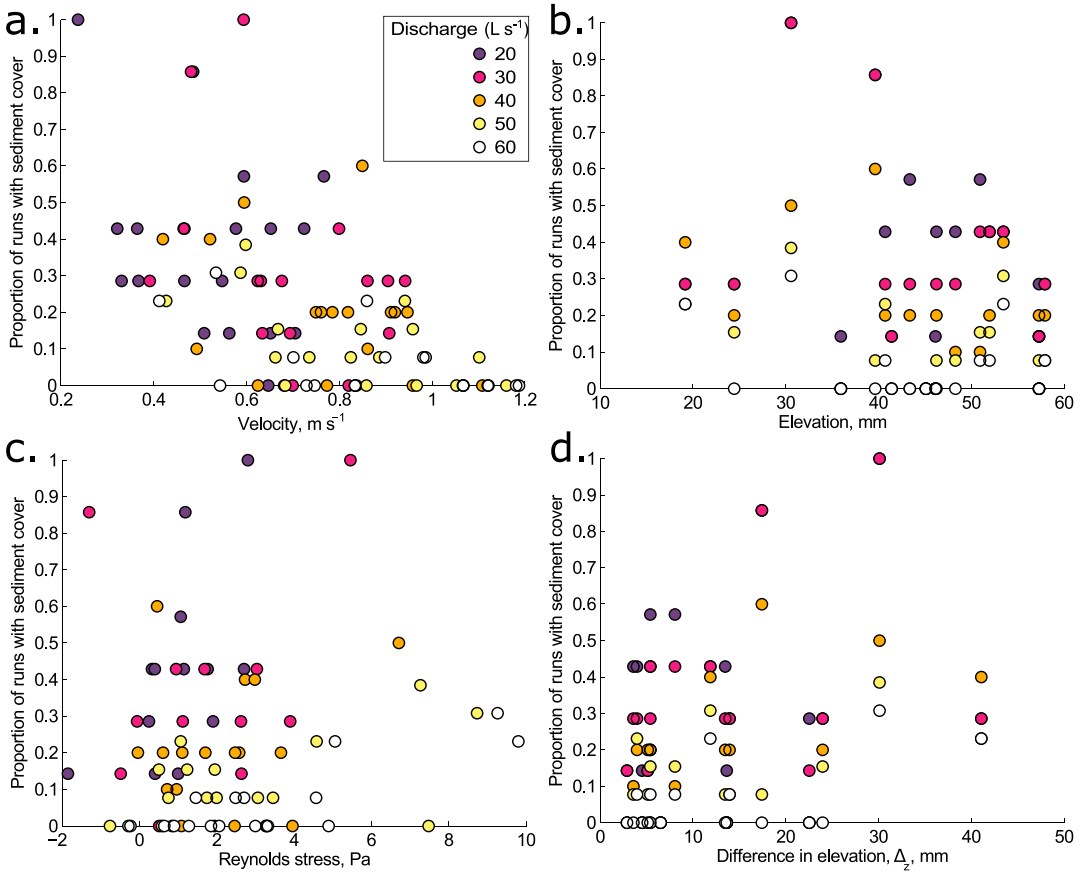

Figure 10. Relationships between flow hydraulics (downstream velocity and Reynolds stress), topographic indices (elevation and Δ_z), and the occurrence of sediment cover at 18 locations across the flume. Hydraulic data are from experimental runs in the companion paper at 20, 30, 40, 50, and 60 L s^{-1} without sediment cover (as shown in Figure 3, right column), whereas the sediment cover data are from the sediment erosion components of the experiments presented here. The two data sets are therefore not strictly comparable, but the hydraulic data gives a useful indication of the likely conditions during the sediment runs. The 18 locations are shown in Figure 3. For the erosional component of each experimental run, we identify whether sediment cover was present at each of the 18 locations when Q was equal to each of the five discharges (20 though to 60 L s^{-1}). The proportion of runs is the number of occurrences of sediment cover over the number of times that those hydraulic conditions occurred.

cover against the five hydraulic and topographic variables only retains velocity ($p < 0.001$), so velocity is the main control. Other variables are not included because of autocorrelation between variables.

Further analysis segmented the data set by discharge and regressed proportion of runs with sediment cover against each of the five variables (Table 1). Each of velocity, Δ_z and Reynolds stress produce significant relationships, primarily at higher discharges. The gradients of the relationships with velocity and Δ_z are as expected (negative and positive respectively; Table 1). However, the relationships with Reynolds stress are positive (Table 1), which is counter to the idea that increased stress would inhibit sediment cover. This result may indicate the influence of a third factor which both increases turbulence and encourages sediment deposition. We therefore consider velocity and Δ_z to be the main controls on sediment cover development. One source of uncertainty in this analysis is the different sediment masses between runs; a lack of sediment cover could result from a lack of sediment supply instead of the hydraulic conditions. Therefore the occurrences of sediment cover are underestimates of what would happen with a continuous sediment supply.

4.7. Sediment Stability Compared to Flatbed Conditions

In order to assess the impact of the bed topography on sediment stability, our data are compared to results in *Hodge et al.* [2016], which used the same uniform sediment as in runs Q20/S4$_C$ and Q20/S4$_F$, but on a flat, plywood, flume bed, onto which a layer of medium sand grains was glued to add roughness. The flatbed

Table 1. Gradients of Linear Regressions Between the Proportions of Runs With Sediment Cover and Five Different Hydraulic and Topographic Variables

	Discharge ($L\,s^{-1}$)				
	20	30	40	50	60
Velocity	−0.56	−0.63	−0.38	−0.34*	−0.23*
Reynolds stress	0.12**	0.04	0.03	0.02*	0.03*
Elevation	−0.00	−0.01	−0.01	−0.00	−0.00
Δ_z	0.01	0.01	0.01*	0.01**	0.01*
σ_z	−0.01	0.00	0.00	0.00	0.01

*$p < 0.1$.
**$p < 0.05$.

experiments took two forms: (1) individual, isolated fine or coarse grains were placed in the center of the flume and the discharge increased until the grains were entrained; and (2) sediment was added to the flume in bulk under steady flow conditions, forming a combination of sediment patches and isolated grains. Discharge was increased until the isolated grains and patches were entrained.

Individual fine and coarse grains on this flatbed moved at respective discharges of 6 and $8\,L\,s^{-1}$. When a pulse of sediment was added to the flume and allowed to form patches, the thresholds for initial sediment entrainment from the patches increased to 11 and $10\,L\,s^{-1}$ for fine and coarse sediment, respectively. Across all experiments with sediment patches, the mean discharge at which grains were entrained from a patch was between 15 and $25\,L\,s^{-1}$. In contrast, in the experiments with the 3-D printed bed, patches of sediment were present in the flume even at an initial discharge of $50\,L\,s^{-1}$. The mean threshold discharge for the erosion of the sediment patches $(\overline{Q_t})$ was between 40 and $60\,L\,s^{-1}$. Furthermore, in the runs with uniform coarse or fine sediment (as used in the flat bed experiments), sediment patches were still stable in the flume at a discharge of $75\,L\,s^{-1}$. This stability demonstrates the importance of bedrock morphology for maintaining sediment cover.

5. Discussion

The discussion addresses each of the research questions in turn, before considering the broader implications for bedrock-alluvial channels and bedrock erosion.

5.1. How Does the Amount of Sediment Cover Vary with Flow Discharge and Supplied Sediment Mass?

The initial sediment cover that forms on the bare bedrock bed after the first 5 min is a linear function of the mass of sediment input to the flume (Figure 2). The relationships between sediment mass and cover for the experiments with different initial discharges have similar gradients but are vertically offset from each other, such that the same sediment mass produces less cover at a higher discharge. Consequently, both sediment mass and initial discharge significantly affect the sediment cover. The linear form of these relationships is similar to those previously proposed from theoretical [*Sklar and Dietrich*, 2004] and flume [*Chatanantavet and Parker*, 2008] analyses. These published relationships used a relative sediment flux (defined as sediment supply over capacity sediment flux) whereas we use a known mass of sediment. Figure 2 could be converted to a flux format by estimating a capacity sediment flux and normalizing the sediment mass by the time it took to feed into the flume. Such a calculation is likely to collapse the different relationships in Figure 2 onto each other but is not undertaken because of the uncertainties around estimating a capacity bed load flux in a bedrock-alluvial channel.

One implication of the use of a single pulse, rather than a constant flux, of sediment is that the experiments represent a dynamic, rather than an equilibrium, condition. At low sediment inputs in these experiments, sediment cover may be underdeveloped compared to what would be produced by even a small, constant flux. In these experiments it is possible to have areas where sediment patches would be stable were they to develop but which were overpassed by the input sediment. With a longer duration sediment feed there would be a greater chance of these areas developing sediment cover. Constant feed conditions may mean that there is less difference in sediment cover between the different sediment inputs than is observed in these experiments, which may further enhance the importance of the bed topography. However, sediment inputs to many bedrock-alluvial channels in upland areas are likely to be episodic and may or may not coincide with high-flow events, so our experimental conditions could be considered to be a more realistic starting point than would be a constant sediment feed rate.

5.2. To What Extent does Bed Topography Control Sediment Patch Location?

Comparison between the locations of initial sediment cover (Figure 4) indicates that sediment is generally, but not exclusively, deposited in areas of the bed that are lower and have a higher Δ_z. As the sediment pulse mass increases, the cover extends to higher elevations and lower Δ_z (Figure 4). The exception to these trends is the 50 L s^{-1} runs. This could be because of changes in local velocity making these areas no longer suitable for sediment deposition, which is supported by the locations for which there is velocity data (seen in Figure 3). Another explanation is that the higher flow velocities mean that the input sediment travels further downstream before it reaches the bed and thus overpasses the deepest areas in the upstream section of the bed. The 50 L s^{-1} results may therefore be more influenced by the experimental boundary conditions than the other runs. Analysis of the length scales of the initial sediment cover shows clustering at small scales at Q20/S2 (Figure 6a), with progressively less clustering at these scales as the amount of sediment cover increases and the distributions become more similar to a random placement of sediment (Figures 6b to 6d). The length scale of the initial clustering is similar to the minimum length scale needed to describe the bed roughness. This identified length scale of 150 mm is likely to reflect the minimum lateral dimension of bed hollows because (1) the bed hollow dimension will constrain the maximum distance between grains in the same sediment patch and (2) in order for σ_z to reach its maximum, the sample window will need to be large enough to include both the base of the hollow and the surrounding high areas. The length scale analysis suggests that at low sediment cover the bed topography is an important control on the spatial distribution of sediment patches. As sediment cover increases, the length scale of the sediment patches become independent of the channel topography.

5.3. To What Extent Does Bed Topography Control Sediment Patch Stability?

The bed topography has been demonstrated to influence the initial location of sediment patches. The latter parts of the experiments with increasing discharge show that this topography is also important for determining sediment patch stability. Furthermore, flatbed experiments with comparable sediment [*Hodge et al*., 2016] show that without bed topography, sediment patches are entrained at far lower discharges. Analysis of the erosion of sediment patches (Figure 7) identified three different regimes; within each regime the experiment showed a similar decrease in sediment cover with increasing discharge, regardless of the discharge at which the experiment was initiated. However, there are still differences between runs within the same regime, indicating that there is also stochasticity in the entrainment process.

The first regime comprised all runs with 2 kg of sediment and run Q35/S4; these runs had the least sediment cover at any discharge (Figure 7a). In these experiments there was not enough sediment to fill all the areas that could hold stable sediment patches at a given discharge. Patch development was therefore supply limited. The length scales of these sediment patches were controlled by the bed topography (Figure 6a).

The 4 kg and 8 kg runs together comprised the second regime, with relatively small differences between the amount of cover during the erosional phase despite the differences in sediment input which led to some differences in initial cover that are quickly eradicated once erosion starts (Figure 7a). The similarities suggest that at any discharge, all potentially stable areas of the bed are filled with sediment and that any excess sediment (particularly in the case of the 8 kg runs) is removed. The interaction between the bed topography and the flow thus provides a template for sediment patch stability. Under this second regime, patch extent is therefore a function of the interaction between the bed and the flow, rather than the amount of sediment supplied.

The final regime is the 16 kg runs, which have disproportionally greater sediment cover during the latter parts of the experiment (Figure 7a). In these runs the large volume of sediment appears to override the influence of the bed topography, with no apparent relationship between the length scales of the sediment patches and the topography (Figure 6). The patches are more extensive and more stable than would be predicted from earlier runs; if topography was the only factor influencing the stability of sediment patches that formed in these areas, then it seems likely that sediment cover would also have formed in runs with less sediment. The increased stability of the sediment patches could be because of grain-grain interactions increasing the critical shear stress for grain entrainment, e.g., through sheltering effects and increased pivoting angles [*Hodge et al*., 2011]. The same increase could be due to the presence of sediment locally increasing the

bed roughness and hence decreasing the ability of the flow to entrain the sediment [e.g., *Johnson,* 2014; *Inoue et al*., 2014]; such an impact of sediment cover on flow was observed by *Hodge and Hoey* [2016]. The idea of grain-grain interactions stabilizing sediment cover is also supported by the observation that this stable cover occurred on higher areas of the bed with lower values of Δ_z (Figure 10), where the higher flow velocities [*Hodge and Hoey*, 2016] might instead be expected to make the sediment patches less stable, rather than the observed increase in stability.

Over these three regimes, the extent of sediment cover changes from being a function of sediment supply when sediment is undersupplied to being a function of the interaction between the bed and the flow and then back to being a function of sediment supply again. On the whole, the volume of the initial sediment input appears to be more important than the discharge at which it is introduced. The only exception is that at high initial discharges sediment may have too much momentum to be deposited in stable locations. Within each regime there also appears to be fairly little memory in the system, with the sediment cover quickly adjusting to the current flow conditions. This is demonstrated by the similarities between the sediment cover erosion curves in Figure 7, which show a similar pattern for runs with the same sediment mass but different initial discharges.

5.4. What Are the Relationships Between Sediment Patch Occurrence, Hydraulics, and Local Bed Topography?

Analysis of the locations where sediment patches formed, and their stability, as they eroded, demonstrated that both bed elevation and Δ_z are important, but not exclusive, controls. The absence of spatially distributed hydraulic data meant that the only possible comparison was with hydraulic data from runs without sediment cover (which neglects the influence that sediment cover has on local velocity). This comparison showed that across all discharges, velocity had the most significant control on the occurrence of sediment cover (Figure 10). At some individual discharges (Table 1), Δ_z and Reynolds stress also had a significant relationship with the occurrence of sediment cover, although the relationship with Reynolds stress was positive rather than negative as expected. These findings to an extent appear to contradict previous studies, in which elevation has been identified as a controlling factor [*Johnson and Whipple*, 2007; *Turowski et al*., 2008].The filling model shows that in this case, infilling the bed produces poor predictions of both the mean elevation and the location of sediment cover (Figure 4), so predictions of sediment cover location need to consider spatial variation in flow velocity.

5.5. Implications for Bedrock-Alluvial Channels

The flume experiments reported in this, and the companion, paper have demonstrated that underlying bedrock topography has significant impacts on the hydraulic and sediment transport processes and relationships that occur within a bedrock-alluvial channel. These processes and relationships are outlined in Figure 11, which is an extension of alluvial channel interaction models [e.g., *Ashworth and Ferguson*, 1986] to bedrock-alluvial systems. Over short timescales and in these experiments, the bedrock morphology can be considered to be fixed. However, over longer timescales and/or extreme events, the bedrock morphology itself is an additional degree of freedom [*Tinkler and Wohl*, 1998].

This and the companion paper have quantified many of the relationships in Figure 11 through demonstrating how a particular bedrock morphology controls sediment patch dynamics by (1) inducing a spatial pattern of flow velocities and consequently (2) providing a template of areas with greater or lesser sediment stability, as well as (3) controlling the relationship between supplied sediment mass and patch area. Each of these relationships changes with discharge. However, the degree to which the form of these relationships is specific to this particular bed remains unknown. The particular combination in the prototype site of relatively rough and smooth upstream and downstream areas, respectively, may maximize the spatial variation in processes compared to other bed morphologies.

The question of how to quantify bedrock morphology in a way that represents its influences on the processes in Figure 11 is unresolved, despite its clear importance in these processes [*Chatanantavet and Parker*, 2008; *Finnegan et al*., 2007; *Johnson and Whipple,* 2007; *Inoue et al*., 2014]. Use of a single roughness length [e.g., *Inoue et al*., 2014; *Johnson*, 2014] is problematic because it varies with the window size over which it is measured (Figure 6e) and is nondirectional. Furthermore, a single length scale does not account for the spatial variation in topography that controls the spatial extent of sediment patches under low and medium sediment supplies. We have demonstrated that one possible approach is to identify the minimum window size that is

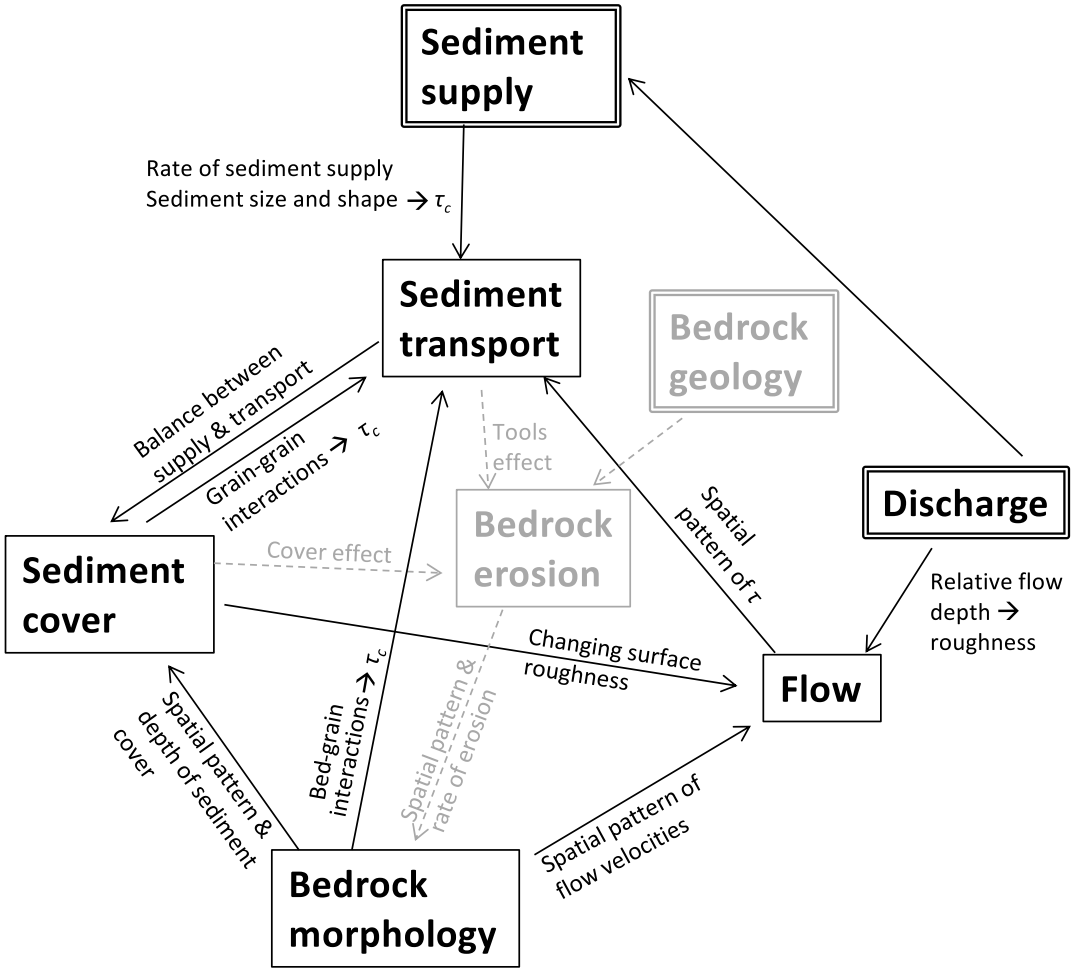

Figure 11. An adaptation of alluvial river process-form interaction models to bedrock-alluvial channels [e.g., *Ashworth and Ferguson*, 1986]. Black arrows indicate interactions over short timescales, grey arrows indicate interactions over time scales at which bedrock incision operates. Boxes with a double outline indicate an external control. This diagram assumes that bedrock incision is caused by sediment transport. Each arrow is labeled with a summary of the processes and factors causing the indicated interaction; processes in black have been addressed in this and the companion paper. τ and τ_c are shear stress and critical shear stress.

needed to capture the bed roughness (defined as σ_z), giving two length scales, a vertical standard deviation of elevations (σ_z), and an additional horizontal length scale (i.e., the minimum window size). In these data, the latter length scale seems to be linked to the size of sediment patches under low supply conditions.

The issue of identifying appropriate roughness scales is hampered by the lack of data on sediment cover and topography from bedrock-alluvial channels. A systematic analysis of such data may allow identification of an appropriate scale at which to measure roughness in order to relate it to sediment patch properties. These data could also help to identify the key factors that control channel roughness, e.g., bedrock properties, abrasion processes, or sediment cover [*Lamb et al.*, 2015] but would also need to account for temporal variations in sediment cover [e.g., *Johnson et al.*, 2009]. Sediment patches in bedrock-alluvial systems are equivalent to bed forms in alluvial channels and have been observed in some cases to have similar forms [e.g., *Hersen*, 2005; *Nittrouer et al.*, 2011] and similarly can be considered to be either forced (i.e., occupying topographic niches) or free (i.e., forming on areas of pseudoplane bed conditions). *Nelson and Seminara* [2012] demonstrate analytically how bed forms develop on a flat bedrock bed, with results comparable to those observed by *Chatanantavet and Parker* [2008], but they do not extend the analysis to beds with a more variable topography, such as in these experiments. Systematic field data would hence enable a classification of bed forms in bedrock-alluvial systems to be developed, such as exists for gravel bed channels [e.g., *Montgomery and*

Buffington, 1997], erosional features in bedrock [*Richardson and Carling*, 2005], and bedrock channel morphology [*Wohl and Merritt*, 2001]. Quantifying bedrock morphology will again be necessary, because results presented here indicate that bed forms will be driven by the bed topography at low sediment supplies and become more similar to alluvial ones at higher sediment fluxes.

Another question that remains to be fully addressed is to identify the conditions under which within-reach variations are an important control on the processes in Figure 11 [*Lague*, 2014]. The companion paper [*Hodge and Hoey*, 2016] demonstrated that even under high flow conditions, there is considerable spatial variation in flow velocity and Reynolds shear stress, with a reach-averaged approach likely to underestimate the magnitude of forces applied to the bed and sediment [*Ferguson*, 2003]. The analysis of sediment cover shows that topographic variation decreases in importance as the amount of sediment in the reach increases. Bed topography will therefore also affect sediment transport at low and intermediate sediment cover, as it will determine the locations of the sediment patches that the sediment grains move between, in the same way that grain movement is controlled by pool-bar spacing in an alluvial channel [*Pyrce and Ashmore,* 2003].

The finding that large amounts of sediment can override other factors in the channel is consistent with previous numerical modeling results [*Lague*, 2010; *Hodge*, 2015] and field data from both bedrock-alluvial and alluvial rivers [e.g., *Cui et al*., 2003; *Turowski et al*., 2012]. Both *Lague's* [2010] and *Hodge's* [2015] models reproduced the development of sediment cover under fluctuating sediment inputs and found that significant sediment cover was produced by occasional large (greater than channel capacity) sediment inputs, which overrode the relationship that was otherwise produced between sediment flux and cover. The flume results presented here demonstrate that similar effects can also occur on a more local basis within the bed. This occurred when areas of extensive sediment cover demonstrated enhanced stability relative to that which would be expected from runs with smaller sediment inputs. None of these runs had complete sediment cover though, indicating that sediment storage and enhanced stability does not only occur when the bed is fully alluvial. These findings have similarity to the relationships between sediment volume and sediment transport derived by *Lisle and Church* [2002] for degrading alluvial rivers. Differences between the flume and model results reflect the importance of interactions between the topography, flow, and sediment transport that are not fully reproduced in either of the previous models.

5.6. Implications for Bedrock Erosion

A relationship between sediment flux and sediment cover is necessary for many models of channel incision. The analysis of the initial sediment cover produced in the flume runs supports the use of a linear relationship, as is already widely used [e.g., *Sklar and Dietrich*, 2004]. However, as already outlined, the single sediment input is not directly equivalent to a constant flux. Furthermore, the analysis of the erosion of the patches and the identification of three different regimes suggests that the relationship may be more complicated and may depend on the magnitudes of flow events and the nature of sediment supply into the reach (i.e., pulsed or continuous; timing relative to flow events). The similarity between the results from the 4 kg and 8 kg runs suggests that under intermediate sediment inputs, sediment cover may actually be insensitive to the exact value. Instead, the bed topography plays an important role in determining the extent of sediment cover that is stable at a given discharge. There is therefore a need to work out how the impact of this subreach heterogeneity can be upscaled for calculations of long-term bedrock incision [*Lague*, 2014]. Such a development will complement advances in understanding how intergranular interactions affect the flux-cover relationship [*Hodge and Hoey*, 2012].

This insensitivity of sediment cover to sediment input is consistent with the theoretical predictions of cover fraction developed by *Inoue et al.* [2014]; they predict that with a topographically rough bed, there is a relatively small change in sediment cover as relative sediment flux increases from just over zero to equal to capacity. In contrast, with a smooth bed, they predict no sediment cover at low fluxes and a rapid increase at higher fluxes. However, *Inoue et al.'s* [2014] relationship for rough beds only applies when the ratio of bed roughness length (e.g., standard deviation of bed elevations) to grain size is 20. In the flume experiments presented here, the ratio has a value of about 2 (σ_z for the entire bed is 12 mm, and D_{50} is 7.3 mm). At a ratio of 2.5 *Inoue et al.* [2014] predict that no sediment cover should form. This again highlights the importance of spatial variability in topographic roughness and the need to address how the roughness and topography of bedrock-alluvial rivers are quantified.

One component of Figure 11 that has not been addressed directly is the processes relating to bedrock erosion. However, sediment cover controls the areas of the bed that can be eroded. It has been observed in the field, flume, and numerical experiments [*Finnegan et al*., 2007; *Johnson and Whipple*, 2007; *Turowski et al*., 2008; *Nelson and Seminara*, 2011] that sediment cover collects in the lowest parts of the bed, meaning that erosion is focussed at higher elevations, potentially widening the channel [*Turowski et al*., 2008; *Yanites and Tucker*, 2010; *Nelson and Seminara*, 2011]. However, sediment does not exclusively collect at low elevations in these experiments (Figure 5), indicating that the pattern of flow may be an important control on the spatial pattern of erosion and hence the morphological evolution of the channel.

6. Conclusion

A 1:10 scale Froude model of a bedrock-alluvial channel was used to measure sediment dynamics on a scaled prototype channel morphology. Our findings are that (1) sediment patches tend to initiate in the lowest areas of the bed, but areas of high flow velocity can inhibit this; (2) at low sediment inputs the extent of sediment patches is determined by the bed topography and can be insensitive to the exact volume of sediment supplied; and (3) at higher sediment inputs more extensive patches are likely stabilized by grain-grain and grain-flow interactions, and there is a lesser influence of the bed topography. These results imply that the bed topography, hydraulics and grain-grain interactions can all be strong influences on the spatial pattern and stability of sediment patches, and hence, the areas of the bed that are protected from erosion and the pathways of bed load transport. The nonlinear interactions between topography, hydraulics, and sediment processes mean that the resulting patterns of hydraulics and sediment cover cannot be easily upscaled to a reach-averaged value. There is therefore a need to develop metrics of channel morphology that account for its spatial influence on hydraulics and sediment processes. The range of initial discharges and sediment input masses used here simulates a range of scales of sediment supply events and a range of ratios of sediment supply to discharge (transport capacity). These results provide further evidence for the significance of the timing and magnitude of sediment supply and flow events in upland rivers.

Acknowledgments
This project was supported by the Royal Geographical Society (with IBG) with a Small Research Grant awarded to R.A.H. Thanks to Kenny Roberts and Tim Montgomery for laboratory assistance. We thank the Editor, AE, Peter Nelson, and two anonymous reviewers for their thorough reviews and useful suggestions. Data are available from the corresponding author by request (rebecca.hodge@durham.ac.uk).

References

Ashworth, P. J., and R. I. Ferguson (1986), Interrelationships of channel processes, changes and sediments in a proglacial braided river, *Geogr Ann A.*, *68*, 361–371.

Chatanantavet, P., and G. Parker (2008), Experimental study of bedrock channel alluviation under varied sediment supply and hydraulic conditions, *Water Resour. Res.*, *44*, W12446, doi:10.1029/2007WR006581.

Cui, Y., G. Parker, T. E. Lisle, J. Gott, M. E. Hansler-Ball, J. E. Pizzuto, N. E. Allmendinger, and J. M. Reed (2003), Sediment pulses in mountain rivers: 1. Experiments, *Water Resour. Res.*, *39*(9), 1239, doi:10.1029/2002WR001803.

Ferguson, R. I. (2003), The missing dimension: Effects of lateral variation on 1-D calculations of fluvial bedload transport, *Geomorphology*, *56*(1–2), 1–14, doi:10.1016/S0169-555X(03)00042-4.

Finnegan, N. J., L. S. Sklar, and T. K. Fuller (2007), Interplay of sediment supply, river incision, and channel morphology revealed by the transient evolution of an experimental bedrock channel, *J. Geophys. Res.*, *112*, F03S11, doi:10.1029/2006JF000569.

Goode, J. R., and E. Wohl (2010), Coarse sediment transport in a bedrock channel with complex bed topography, *Water Resour. Res.*, *46*, W11532, doi:10.1029/2009WR008135.

Hersen, P. (2005), Flow effects on the morphology and dynamics of aeolian and subaqueous barchan dunes, *J. Geophys. Res.*, *110*, F04S07, doi:10.1029/2004JF000185.

Hodge, R. A. (2015), Sediment processes in bedrock-alluvial rivers: Research since 2010 and modelling the impact of fluctuating sediment supply on sediment cover, paper presented at Gravel Bed Rivers 8: Gravel Bed Rivers and Disasters, Kyoto and Takayama, Japan, 14–18 Sept. [Available at https://www.youtube.com/watch?v=lDHBvasrAKY.]

Hodge, R. A., and T. B. Hoey (2012), Upscaling from grain-scale processes to alluviation in bedrock channels using a cellular automaton model, *J. Geophys. Res.*, *117*, F01017, doi:10.1029/2011JF002145.

Hodge, R. A., and T. B. Hoey (2016), A Froude-scaled model of a bedrock-alluvial channel reach: 1. Hydraulics, *J. Geophys. Res. Earth Surf.*, *121*, doi:10.1002/2015JF003706.

Hodge, R. A., T. B. Hoey, and L. S. Sklar (2011), Bed load transport in bedrock rivers: The role of sediment cover in grain entrainment, translation and deposition, *J. Geophys. Res.*, *116*, F04028, doi:10.1029/2011JF002032.

Hodge, R., T. Hoey, G. Maniatis, and E. Leprêtre (2016), Formation and erosion of sediment cover in an experimental bedrock-alluvial channel, *Earth Surf. Process Landforms*, *41*, 1409–1420, doi:10.1002/esp.3924.

Huda, S. A., and E. E. Small (2014), Modeling the effects of bed topography on fluvial bedrock erosion by saltating bed load, *J. Geophys. Res. Earth Surf*, *119*, 1222–1239, doi:10.1002/2013JF002872.

Inoue, T., N. Izumi, Y. Shimizu, and G. Parker (2014), Interaction among alluvial cover, bed roughness, and incision rate in purely bedrock and alluvial-bedrock channel, *J. Geophys. Res. Earth Surf.*, *119*, 2123–2146, doi:10.1002/2014JF003133.

Johnson, J. P., and K. X. Whipple (2007), Feedbacks between erosion and sediment transport in experimental bedrock channels, *Earth. Surf. Process Landforms*, *32*(7), 1048–1062, doi:10.1002/esp.1471.

Johnson, J. P. L. (2014), A surface roughness model for predicting alluvial cover and bed load transport rate in bedrock channels, *J. Geophys. Res. Earth Surf*, *119*, 2147–2173, doi:10.1002/2013JF003000.

Johnson, J. P. L., and K. X. Whipple (2010), Evaluating the controls of shear stress, sediment supply, alluvial cover, and channel morphology on experimental bedrock incision rate, *J. Geophys. Res.*, *115*, F02018, doi:10.1029/2009JF001335.

Johnson, J. P. L., K. X. Whipple, L. S. Sklar, and T. C. Hanks (2009), Transport slopes, sediment cover, and bedrock channel incision in the Henry Mountains, Utah, *J. Geophys. Res.*, *114*, F02014, doi:10.1029/2007JF000862.

Krumbein, W. C. (1941), Measurement and geological significance of shape and roundness of sedimentary particles, *J. Sediment. Res.*, *11*(2), 64–72.

Lague, D. (2010), Reduction of long-term bedrock incision efficiency by short-term alluvial cover intermittency, *J. Geophys. Res.*, *115*, F02011, doi:10.1029/2008JF001210.

Lague, D. (2014), The stream power river incision model: Evidence, theory and beyond, *Earth Surf. Process Landforms*, *39*(1), 38–61, doi:10.1002/esp.3462.

Lamb, M. P., W. E. Dietrich, and L. S. Sklar (2008), A model for fluvial bedrock incision by impacting suspended and bed load sediment, *J. Geophys. Res.*, *113*, F03025, doi:10.1029/2007JF000915.

Lamb, M. P., N. J. Finnegan, J. S. Scheingross, and L. S. Sklar (2015), New insights into the mechanics of fluvial bedrock erosion through flume experiments and theory, *Geomorphology*, *244*, 33–55, doi:10.1016/j.geomorph.2015.03.003.

Lisle, T. E., and M. Church (2002), Sediment transport-storage relations for degrading, gravel bed channels, *Water Resour. Res.*, *38*(11), 1219, doi:10.1029/2001WR001086.

Montgomery, D. R., and J. M. Buffington (1997), Channel-reach morphology in mountain drainage basins, *Geol. Soc. Am. Bull.*, *109*(5), 596–611, doi:10.1130/0016-7606(1997)109<0596:CRMIMD>2.3.CO;2.

Nelson, P. A., and G. Seminara (2011), Modeling the evolution of bedrock channel shape with erosion from saltating bed load, *Geophys. Res. Lett.*, *38*, L17406, doi:10.1029/2011GL048628.

Nelson, P. A., and G. Seminara (2012), A theoretical framework for the morphodynamics of bedrock channels, *Geophys. Res. Lett.*, *39*, L06408, doi:10.1029/2011GL050806.

Nelson, P. A., M. B. Pittaluga, and G. Seminara (2014), Finite amplitude bars in mixed bedrock-alluvial Channels, *J. Geophys. Res. Earth Surf*, *119*, 566–587, doi:10.1002/2013JF002957.

Nittrouer, J. A., D. Mohrig, M. A. Allison, and A.-P. B. Peyret (2011), The lowermost Mississippi River: A mixed bedrock-alluvial channel, *Sedimentology*, *58*(7), 1914–1934, doi:10.1111/j.1365-3091.2011.01245.x.

O'Connor, J. E., J. F. Mangano, S. W. Anderson, J. R. Wallick, K. L. Jones, and M. K. Keith (2014), Geologic and physiographic controls on bed-material yield, transport, and channel morphology for alluvial and bedrock rivers, western Oregon, *Geol. Soc. Am. Bull.*, *126*, 377–397, doi:10.1130/B30831.1.

Pyrce, R. S., and P. E. Ashmore (2003), The relation between particle path length distributions and channel morphology in gravel-bed streams: A synthesis, *Geomorphology*, *56*(1–2), 167–187, doi:10.1016/S0169-555X(03)00077-1.

Richardson, K., and P. A. Carling (2005), A typology of sculpted forms in open bedrock channels, *Geol. Soc. Am. Special Pap.*, *392*, 1–108, doi:10.1130/0-8137-2392-2.1.

Scheingross, J. S., F. Brun, D. Y. Lo, K. Omerdin, and M. P. Lamb (2014), Experimental evidence for fluvial bedrock incision by suspended and bedload sediment, *Geology*, *42*, 523–526, doi:10.1130/G35432.1.

Sklar, L. S., and W. E. Dietrich (2004), A mechanistic model for river incision into bedrock by saltating bed load, *Water Resour. Res.*, *40*, W06301, doi:10.1029/2003WR002496.

Tinkler, K., and E. Wohl (1998), A primer on bedrock channels, in *Rivers Over Rock: Fluvial Processes in Bedrock Channels*, edited by K. J. Tinkler and E. E. Wohl, pp. 1–18 , AGU, Washington, D. C.

Turowski, J. M., N. Hovius, H. Meng-Long, D. Lague, and C. Men-Chiang (2008), Distribution of erosion across bedrock channels, *Earth Surf. Process Landforms*, *33*(3), 353–363, doi:10.1002/esp.1559.

Turowski, J. M., A. Badoux, J. Leuzinger, and R. Hegglin (2012), Large floods, alluvial overprint, and bedrock erosion, *Earth Surf. Process Landforms*, *38*, 947–958, doi:10.1002/esp.3341.

Whitbread, K., J. Jansen, P. Bishop, and M. Attal (2015), Substrate, sediment, and slope controls on bedrock channel geometry in postglacial streams, *J. Geophys. Res. Earth Surf.*, *120*, 779–798, doi:10.1002/2014JF003295.

Wohl, E. E., and D. M. Merritt (2001), Bedrock channel morphology, *Geol. Soc. Am. Bull.*, *113*(9), 1205–1212.

Yanites, B. J., and G. E. Tucker (2010), Controls and limits on bedrock channel geometry, *J. Geophys. Res.*, *115*, F04019, doi:10.1029/2009JF001601.